Received: 21 October 2025 | Revised: 14 March 2026 | Accepted: 30 March 2026

DOI: 10.1002/cjce.70415

SPECIAL ISSUE ARTICLE

THE CANADIAN JOURNAL OF CHEMICAL ENGINEERING

Thermophysical properties applied to chemical engineering 1990–2025 in ESIQIE-IPN: A high-pressure thermodynamics perspective

Luis A. Galicia-Luna[†]

Laboratorio de Termodinámica, S.E.P.I.-E.S.I.Q.I.E. Instituto Politécnico Nacional, UPALM, Lindavista, México

Correspondence
Luis A. Galicia-Luna, Laboratorio de Termodinámica, S.E.P.I.-E.S.I.Q.I.E. Instituto Politécnico Nacional, UPALM, Edif. Z, Secc. 6, 1ER piso, Lindavista C.P. 07738, México D. F., México.
Email: lgalicial@ipn.mx

Funding information
National Polytechnic Institute; CONACyT

Abstract

Over the last three decades, the High-Pressure Thermodynamics Laboratory at ESIQIE-IPN has generated high-accuracy thermophysical-property data and contributed to the development and assessment of equations of state and molecular models for systems relevant to national and international chemical engineering. The discussion is organized around six interconnected research lines: (I) high-pressure phase equilibria of pure fluids and mixtures; (II) volumetric properties (*PvT*); (III) solubility and solid–liquid–gas equilibria in supercritical fluids; (IV) high-pressure viscosities; (V) gas hydrate phase equilibria; and (VI) equations of state supported by molecular simulation. For each line, we highlight methodological innovations, experimental challenge, solutions, and representative case studies that illustrate how measurements and modelling were combined. We also discuss the scientific, academic, and emerging industrial impact of this work, including special issues in international journals, collaborative developments in equations of state, and applications in supercritical extraction and hydrate-based separation processes. Finally, we outline open challenges for thermodynamics in chemical engineering, particularly regarding accurate descriptions of the critical region, compressed liquids, and environmentally benign separation processes.

KEYWORDS

equations of state, gas hydrates, high-pressure, phase equilibria, supercritical fluids, thermophysical properties

Abbreviations: ESIQIE, higher school of chemical engineering and extractive industries; HPLC, high-performance liquid chromatographs; IPN, National Polytechnic Institute; LLVE, liquid–liquid–vapour equilibrium; NRTL, non random two liquids; OF, objective function; PvT, volumetric properties; SCFE, supercritical fluid extraction; SEPI, graduate studies and research section; SF, supercritical fluids; SLE, solid–liquid equilibrium; SLGE, solid–liquid–gas equilibrium; SLVE, solid–liquid–vapour equilibrium; VLE, vapour–liquid equilibrium; VTD, vibrating tube densimeter.

[†]Emeritus National Researcher, Member of the Mexican Academy of Sciences and Doctor Honoris Causa.

This article has been published as part of the "100 Years of Chemical Engineering in Mexico" special issue/section.

1 | INTRODUCTION

Accurate thermophysical properties are essential for the design, optimization, and safe operation of processes in the chemical, petroleum, environmental, and food industries.[1,2] Vapour–liquid and liquid–liquid equilibria, volumetric properties, transport properties, and hydrate phase equilibria at elevated pressures provide the basis for equipment design, process simulation, and scale-up.[3] Over the last 40 years, the development of high-pressure thermodynamics has been closely linked to advances in

equations of state, molecular simulation and experimental techniques capable of delivering reliable data with quantified uncertainties.

In Mexico, the establishment of a high-pressure thermodynamics laboratory dedicated to chemical engineering problems filled a significant gap: until the late 1980s, there was no national facility systematically generating high-quality thermophysical data for industrially relevant systems. Motivated by this need, the High-Pressure Thermodynamics Laboratory at the Graduate Studies and Research Section (SEPI) of ESIQIE-IPN was conceived in the early 1990s and became operational in 1997. Since then, the laboratory has focused on producing accurate experimental data and developing models for systems involving supercritical fluids, complex mixtures, and hydrate-forming components, while training a new generation of specialists in thermodynamics.[1–9]

The evolution of the High Pressure Thermodynamics Laboratory serves to analyze the progress of research on thermophysical properties between 1990 and 2025, and its contribution to chemical engineering in Mexico. The analysis is based on scientific issues, methodological innovations, and representative case studies, and is briefly summarized in historical context when useful for understanding the development of the research objectives.

2 | EVOLUTION OF RESEARCH LINES AND METHODOLOGICAL DEVELOPMENT

Since its creation, the laboratory has pursued six main, interconnected research lines: (I) high-pressure phase equilibria of pure fluids and mixtures; (II) volumetric properties (PvT) of pure compounds and complex mixtures; (III) solubility and solid–liquid–gas equilibria in supercritical fluids; (IV) high-pressure dynamic viscosities; (V) hydrate phase equilibria and dissociation conditions; and (VI) development of equations of state and molecular-based models. These lines evolved in parallel, with each new experimental or modelling capability enabling more complex systems and applications. Below, we summarize this evolution and highlight how experimental and theoretical efforts were integrated.

2.1 | High-pressure phase equilibria

The first priority of the laboratory was to obtain accurate vapour–liquid equilibrium (VLE) and critical data for systems involving carbon dioxide and light alcohols,[10] motivated by their relevance in supercritical extraction and in the design of separation units. Early work focused on CO_2 + ethanol and CO_2 + 1 − propanol mixtures over wide temperature and pressure ranges using a static–analytical method with sapphire-window cells.[11,12] These data is part of systematic study of CO_2 + alcohols and provided a basis for developing and validating cubic equations of state combined with excess-Gibbs-energy mixing rules, such as the Patel–Teja[13] equation with extended Wong–Sandler mixing rules.[14]

As the experimental infrastructure matured, the program expanded towards multicomponent mixtures and systems relevant to hydrate formation, gas processing and environmental separations. The same static–analytical methodology, later coupled with vibrating-tube densimeter, enabled the simultaneous determination of phase compositions and saturation densities, which is particularly valuable for the calibration and assessment of advanced equations of state.[15]

2.2 | Volumetric properties of pure fluids and mixtures

Volumetric properties (PvT) at high pressures are required for the design of equipment and the implementation of energy-efficient processes. Based on the author's experience during his doctoral work in Paris,[16,17] the laboratory developed several vibrating-tube densimeter (VTD) setups for pressures up to 25 MPa and temperatures up to about 363 K.[18,19] These systems were designed to minimize systematic errors through careful calibration, on-line data acquisition and tight thermal control. Systematic studies were performed for pure and their mixture with alcohols,[19,20] alkanes[21,22] and water[23,24] and sulphur-containing compounds,[25,26] motivated by applications in refining, solvent selection, and water treatment.

2.3 | Solubility and supercritical fluid extraction

Another major research line addressed the solubility of solids and heavy organics in supercritical CO_2 and other supercritical solvents, targeting separation processes with reduced environmental impact. Using static–analytical[27] and dynamic–analytical methods,[28] the laboratory determined solubilities of thiophene derivatives,[29] carotenoids,[30] boldine,[31] vanilla components,[32,33] limonene,[34] and squalene,[35,36] among others, in supercritical CO_2 and CO_2 + co-solvent mixtures.[37,38] These data were combined with empirical and semi-predictive models to support the design of supercritical extraction

units for natural products and for the removal of contaminants.

2.4 | High-pressure viscosity measurements

Transport properties, such as dynamic viscosity, are fundamental for pipeline design, enhanced oil recovery, and complex fluid modelling.[39,40] The laboratory developed high-pressure capillary viscometers to simultaneously determine viscosity and density up to 70 MPa and 423 K.[41,42] Two viscometers were used: (1) a straight-tube viscometer, which uses the Hagen–Poiseuille equation,[42] and (2) a coil-type capillary viscometer, which uses a modified Hagen–Poiseuille equation for Newtonian fluids.[43] These were used to study alkanes,[44,45] alcohols,[46] and polar solvents,[47] with the aim of proposing accurate empirical models for use in process simulators.

2.5 | Gas hydrate phase equilibria

Gas hydrates constitute both an operational challenge and a technological opportunity in the oil and gas industry and in water treatment.[48] Starting in 2012, the laboratory developed isochoric high-pressure cells with vacuum-insulated thermal control for the determination of hydrate dissociation conditions of CO_2 + water systems in the presence of thermodynamic promoters and inhibitors.[49–51] The design minimized equilibration times while allowing for series of visual and non-visual cells to be operated in parallel, increasing throughput and enabling systematic studies of promoters and inhibitors such as tetra-n-butylammonium bromide (TBAB)[51] and tetrahydrofuran (THF).[52]

2.6 | Equations of state and molecular simulation

In parallel with experimental developments, the laboratory worked on equations of state for complex fluids, starting from cubic equations[53,54] with new mixing rules[55–57] and progressing towards SAFT-type[58] and molecular-potential-based models.[59] Particular emphasis was placed on short-range square-well[60] and triangular-well potentials,[61] for which Barker–Henderson[62–64] perturbation theory was extended up to fourth order and combined with Monte Carlo and molecular dynamics simulations.[65] The resulting equations of state were assessed against simulation data for thermodynamic properties and phase boundaries, providing insights into how short-range interactions control critical behaviour and compressed-liquid properties.[59,61]

3 | EXPERIMENTAL INFRASTRUCTURE AND METHODOLOGICAL INNOVATIONS

A detailed description of all experimental devices of the Thermodynamics Laboratory, including calibration procedures and uncertainty analyses,[4] has been reported elsewhere. Table 1 summarizes the thermophysical properties determined in this work for the corresponding experimental system. Most of the equipment was developed and/or modified in the laboratory. All experimental

TABLE 1 Overview of the different experimental facilities of the high-pressure thermodynamics laboratory.

Experimental method	Method	*P* (MPa)	*T* (K)	Year
VLE (P, T, x, y)	Analytical	60	313–673	1996
VLE $(P, T, x, y, \rho^{Liq}, \rho^{Vap})$	Analytical—VTD	30	313–473	2006
PvT	Synthetic—Visual	25	313–473	2000
VTD – PvT (Solubility)	Synthetic—Visual	25	313–473	2002
VTD	Synthetic	140	260–473	1996
Solubility	Analytical	40	278–473	2002
Solubility – PvT	Synthetic	60	263–423	2004
Hydrates	Synthetic-static (visual, non-visual)	40	260–373	2012
Viscosities	Capillary flow (Straight, Coil)	50	283–473	2015
SCFE	Analytical—dynamic	60	308–423	2000
VLE (Plow, T, x, y)	Analytical—dynamic	0.1[a]	298–353	2010
Viscosities	Capillary flow	0.1[a]	298–353	2010

Abbreviations: PvT, volumetric properties; VLE, vapour–liquid equilibrium; VTD, vibrating tube densimeter.

[a]These experimental devices operate at pressures close to the atmosphere.

studies are based primarily on three stages[15,26,33,46,51]: a calibration method against standards, real-time data acquisition (experimental determination), and uncertainty assessment.

Pressure transducers are calibrated against a dead-weight tester with an accuracy on the order of 0.005% of full scale, while temperature is traced to a water triple-point cell and secondary standards. Densities and viscosities are assessed via vibrating-tube densimeters and capillary viscometers, respectively, with gravimetric composition control using a comparator balance and class E1 mass standards. For hydrate and phase-equilibrium measurements, isochoric and static–analytical cells with sapphire windows allow visual inspection, micro-sampling, and coupling to chromatographic analysis when required. The systematic application of these procedures enables the reporting of combined expanded uncertainties for each property, which is essential for model validation and data-bank inclusion.

From a methodological point of view, the main innovations include: (I) adaptation of vibrating-tube densimeter to complex mixtures and high pressures; (II) development of coil-type capillary viscometers for simultaneous density and viscosity measurements; (III) design of visual static–analytical cells combined with chromatographic analysis for low solubilities in supercritical CO_2; and (IV) implementation of compact, vacuum-insulated hydrate cells that significantly reduce equilibration times. In the following section, these advances are illustrated through representative case studies.

4 | REPRESENTATIVE CASE STUDIES

To illustrate the interplay between experimental work, modelling efforts, and process-oriented questions, this section summarizes several case studies carried out in the laboratory. These examples show how individual measurements fit into broader research themes rather than being isolated experiments.

The materials used in this work, their purity, CAS number, and suppliers are detailed in Table 2. All chemicals were used as received, without further purification. Liquid hydrocarbons, 1-propanol, lauric acid, TBAB, and THF were degassed by vacuum stirring before use, while carbon dioxide was used as received.

The water content was determined using a Karl Fischer coulometer (Metrohm 831),[4] resulting in the following mass fractions: hexane 7.06×10^{-4}, decane 4.59×10^{-4}, tetradecane 6.79×10^{-4}, TBAB 5.03×10^{-4}, lauric acid 5.51×10^{-4}, 1-propanol 6.63×10^{-4}, and THF 9.24×10^{-4}.

All experimental apparatus and procedures used have been previously described for Galicia et al.[4] The apparatus used in this work corresponds to five of the experimental facilities available in the laboratory.

4.1 | Vapour–liquid equilibria and criticality of CO_2 + 1-propanol

The binary system $CO_2\,(1) + 1 - \text{propanol}\,(2)$ show in Figure 1, this system is prototypical for supercritical extraction[12] and hydrate inhibition.[50,51]

VLE data and critical points for the binary mixture are reported in Table 3 at 352.83 K, static–analytical measurements were performed to obtain vapour–liquid equilibrium compositions and the binary critical point up to approximately 13 MPa.

The data were correlated with the Patel–Teja[13] equation of state combined with the extended Wong–Sandler[14] mixing rule using the non random two liquids (NRTL) model for the excess Gibbs free energy; in Table 4, are reported the parameters of NRTL model correlated to the binary mixture $CO_2\,(1) + 1 - \text{Propanol}\,(2)$ at 352.83 K.

TABLE 2 Chemical information (supplier, CAS number, and purity by mass fraction).

Compound	Source	CAS. No.	Mass fraction purity[a]
CO_2	Infra Air Products	124-38-9	0.99995
H_2O	Sigma-Aldrich	7732-18-5	0.9995
TBAB	Sigma-Aldrich	1643-19-2	0.9980
Tetradecane	Sigma-Aldrich	629-59-4	0.9970
Lauric Acid	Sigma-Aldrich	143-07-7	0.9870
1-Propanol	Sigma-Aldrich	71-23-8	0.9950
Hexane	Sigma-Aldrich	110-54-3	0.9670
Decane	Sigma-Aldrich	124-18-5	0.9950
THF	J.T. Baker	109-99-9	0.9980

[a]Analysis method: gas chromatography is provided by the manufacturer.

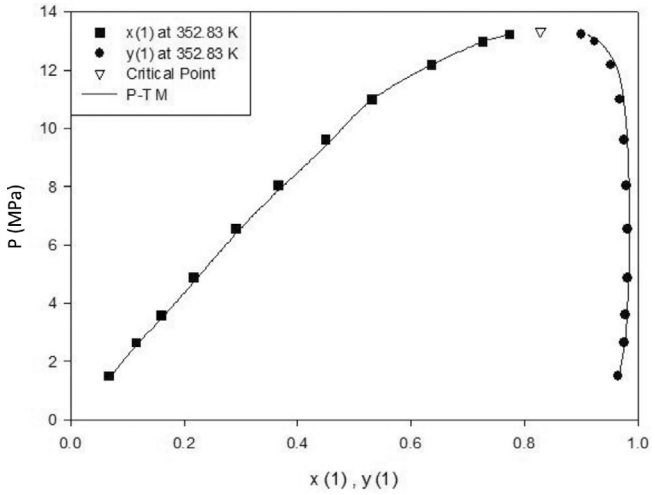

FIGURE 1 Vapour–liquid equilibria and critical point for the binary mixture: CO_2 (1) + 1 − Propanol (2) at 352.83 K: (■) molar liquid fraction this work, (●) molar vapour fraction this work, (−) solid line represents the P-TM EoS.

TABLE 3 Experimental VLE and critical point for the binary mixture CO_2 (1) + 1 − Propanol (2) at 352.83 K.

P (MPa)	x (1)	y (1)
1.49	0.067	0.965
2.65	0.115	0.975
3.59	0.159	0.978
4.86	0.216	0.981
6.55	0.291	0.981
8.04	0.367	0.979
9.61	0.450	0.975
10.99	0.532	0.968
12.17	0.636	0.953
12.97	0.727	0.924
13.22	0.774	0.900
13.33	0.828	0.828[C]

Note: Standard uncertainties u are $u(P) = 0.01\,MPa$ and $u(T) = 0.015\,K$. The relative expanded uncertainty ($k = 2$) is estimated to be $Ur(x) = Ur(y) = 0.0194$.

Binary interaction parameters were fitted through minimization of an objective function based on vapour-phase compositions. The resulting average deviations in pressure and vapour composition confirm that the $P - T - x$ behaviour of this highly non-ideal mixture can be captured reliably with a cubic equation of state when appropriately parameterized.[49–51]

Beyond providing a consistent data set, this study exemplifies the laboratory's general strategy: combining accurate high-pressure measurements with flexible, physically motivated models and using binary systems as building blocks for more complex mixtures relevant to supercritical extraction and hydrate-forming processes, in Table 5, are reported the deviations in pressure and compositions.

TABLE 4 Parameters of NRTL model correlated to the binary mixture CO_2 (1) + 1 − Propanol (2) at 352.83 K.

G^{ex} NRTLModel	k_{12}	τ_{12} (cal/mol)	τ_{21}(cal/mol)
$\alpha_{12} = 0.396$	0.369	537.38	−58.50

Abbreviation: NRTL, non random two liquids.

TABLE 5 Percentage deviation for pressure and composition.

Model G^{ex}	%error P	%error $y(1)$
NRTL	3.02	0.39

Abbreviation: NRTL, non random two liquids.

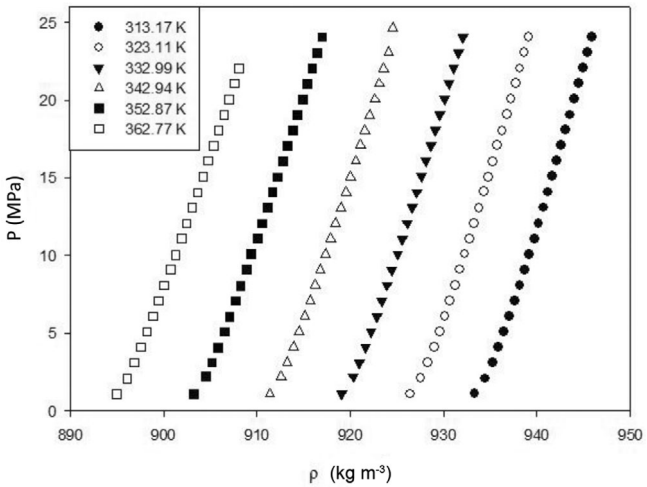

FIGURE 2 Density for a H_2O (1) + 1 − Propanol (2) mixture with $x(1) = 0.9117$, at $T = (313.17, 323.11, 332.99, 342.94, 352.87,$ and $362.77)$ K.

4.2 | Densities of water +1-propanol mixtures and empirical correlations

In Figure 2, presented high-pressure densities of water (1) + 1 − propanol (2) mixtures were measured at several temperatures between roughly 313 and 363 K and pressures up to about 24 MPa for a composition close to $x_1 = 0.912$, the experimental data are reported.

The experimental data, Table 6, show the expected trends: at fixed temperature, density increases with pressure, whereas at fixed pressure, density decreases with temperature. These measurements were correlated with a simple empirical five-parameter model, yielding absolute average percentage deviations on the order of 0.02% and maximum deviations below about 0.03%. Such performance is comparable to or better than other empirical correlations used in engineering practice.[10–12]

TABLE 6 Density for a H_2O (1) + 1 − Propanol (2) mixture with $x(1) = 0.9117$ in mol fraction, at $T = (313.17, 323.11, 332.99, 342.94, 352.87,$ and $362.77)$ K.

$T = 313.17$ K		$T = 323.11$ K		$T = 332.99$ K		$T = 342.94$ K		$T = 352.87$ K		$T = 362.77$ K	
P (MPa)	ρ (kg/m³)	P (MPa)	ρ (kg/m³)	P (MPa)	ρ (kg/m³)	P (MPa)	ρ (kg/m³)	P (MPa)	ρ (kg/m³)	P (MPa)	ρ (kg/m³)
1.09	933.31	1.08	926.44	1.10	919.10	1.09	911.37	1.07	903.24	1.07	894.96
2.08	934.48	2.10	927.55	2.20	920.30	2.20	912.58	2.20	904.50	2.08	896.06
3.10	935.26	3.09	928.31	3.10	921.00	3.09	913.26	3.10	905.18	3.09	896.88
4.07	935.90	4.07	928.97	4.08	921.65	4.10	913.92	4.08	905.84	4.09	897.57
5.08	936.50	5.09	929.58	5.08	922.24	5.08	914.52	5.08	906.50	5.09	898.24
6.09	937.08	6.10	930.13	6.07	922.86	6.10	915.13	6.07	907.09	6.08	898.88
7.07	937.61	7.09	930.67	7.08	923.40	7.09	915.75	7.07	907.69	7.07	899.48
8.08	938.16	8.07	931.22	8.09	923.95	8.09	916.27	8.05	908.26	8.07	900.07
9.09	938.68	9.09	931.77	9.07	924.48	9.08	916.80	9.09	908.88	9.08	900.76
10.08	939.20	10.09	932.27	10.08	925.07	10.09	917.37	10.09	909.40	10.04	901.29
11.08	939.71	11.08	932.80	11.06	925.56	11.08	917.91	11.07	910.05	11.08	901.93
12.06	940.18	12.07	933.30	12.07	926.10	12.09	918.42	12.05	910.57	12.06	902.47
13.08	940.70	13.07	933.79	13.09	926.63	13.08	919.00	13.08	911.11	13.07	903.08
14.07	941.18	14.08	934.29	14.08	927.13	14.08	919.52	14.07	911.66	14.05	903.65
15.08	941.68	15.05	934.78	15.07	927.63	15.06	920.03	15.04	912.21	15.05	904.21
16.07	942.16	16.05	935.28	16.07	928.13	16.07	920.58	16.07	912.80	16.09	904.76
17.08	942.62	17.07	935.78	17.06	928.65	17.09	921.09	17.08	913.29	17.06	905.33
18.06	943.07	18.04	936.26	18.06	929.13	18.05	921.59	18.06	913.83	18.06	905.88
19.05	943.56	19.08	936.76	19.06	929.60	19.04	922.08	19.04	914.34	19.06	906.45
20.05	944.00	20.06	937.21	20.06	930.09	20.05	922.61	20.05	914.91	20.04	907.00
21.09	944.48	21.08	937.71	21.07	930.59	21.06	923.10	21.04	915.40	21.07	907.57
22.05	944.92	22.03	938.17	22.04	931.10	22.00	923.59	22.06	915.92	22.05	908.08
23.05	945.38	23.06	938.64	23.05	931.60	23.05	924.12	23.02	916.45		
24.07	945.87	24.06	939.12	24.04	932.06	24.63	924.57	24.07	916.97		

Note: The relative standard uncertainty is estimated to be $ur(xi) = 0.0007$; the combined uncertainties uc are $uc(P) = 0.010$ MPa and $uc(T) = 0.012$ K; the relative combined expanded uncertainty with a 0.95 level of confidence ($k = 2$) for the density is $U_{rc}\left(\rho_{exp}\right) = 0.002$ kg/m³.

Additionally, Figure 3 shows the deviation between the experimental density and the calculated density data for binary system. From a methodological perspective, this case illustrates how relatively simple correlations, when calibrated with high-quality data, can provide compact yet accurate representations for process simulators and for the tuning of more fundamental equations of state. It also demonstrates the importance of detailed uncertainty analysis for assessing model performance.

4.3 | Solubility of lauric acid in supercritical CO_2 and SLG equilibria

Lauric acid, a major component of coconut oil, is widely used in the food and pharmaceutical industries.[33,36,70] Its solubility in supercritical CO_2 and the associated solid–liquid–gas (SLG) equilibria at high pressures are therefore relevant for supercritical extraction processes.[27–38,70] Using static–synthetic, measured lauric acid solubilities at 308 K and pressures up to about 20 MPa, reported in Table 7.

Figure 4 shows that, at constant temperature, solubility increases with increasing pressure. The data measured in this work are compared with data from the literature and show good agreement[70] between both data sets.

Dynamic–analytical methods using the SLG equilibrium envelope are present in Figure 5 and reported in Table 8. The data confirm that, at constant temperature, solubility increases with pressure.

These measurements form part of a broader program on supercritical extraction, which includes thiophene derivatives,[29] carotenoids,[30] boldine,[31] vanilla components,[32,33] limonene,[34] and squalene.[35,36]

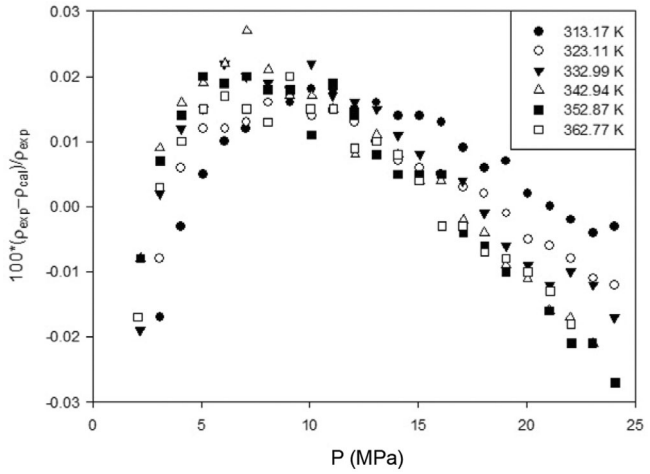

FIGURE 3 Deviations between experimental and calculated density data for a $H_2O\,(1)+1-\text{Propanol}\,(2)$ mixture with $x(1)=0.9117$ using the Galicia-Luna model, at $T=(313.17, 323.11, 332.99, 342.94, 352.87,$ and $362.77)$ K.

TABLE 7 Solubility of lauric acid in supercritical CO_2 at 308 K.

P (MPa)	y_2 (mol mol$^{-1}\times10^{-3}$)
10.16	4.95
13.24	7.22
15.18	10.31
20.46	15.62

Note: Standard uncertainties u are $u(P)=0.01$ MPa and $u(T)=0.015$ K. The relative expanded uncertainty ($k=2$) is estimated to be $\text{Ur}(y)=0.0226$.

Together, these data sets support the design and optimization of environmentally friendlier extraction processes, where CO_2 replaces or reduces the use of organic solvents. The lauric acid system is particularly valuable as a benchmark for model development and for testing the ability of equations of state and semi-empirical correlations to describe solid solubilities.[37,70]

4.4 | Dynamic viscosities at high pressures

Dynamic viscosities of selected pure liquids were measured using high-pressure capillary-flow devices. For example, viscosities of representative organic liquids were determined at temperatures around 297 K up to approximately 29 MPa and at 313 K up to about 30 MPa, are reported in Table 9 measurements liquid dynamic viscosity of CO_2 at 296.72 K.

As expected, the Figure 6 show, viscosity increases with pressure at constant temperature and decreases with temperature at constant pressure. Standard uncertainties were reported for both viscosity and pressure.

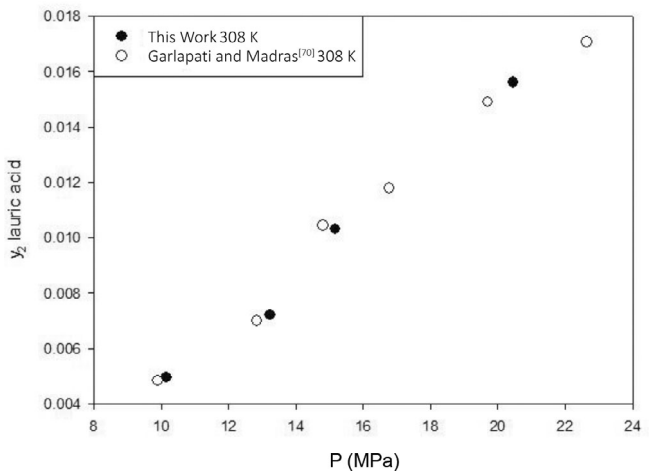

FIGURE 4 Solubility of lauric acid (y_2) in supercritical CO_2 at 308 K: ● This work; ○ Garlapati and Madras.[70]

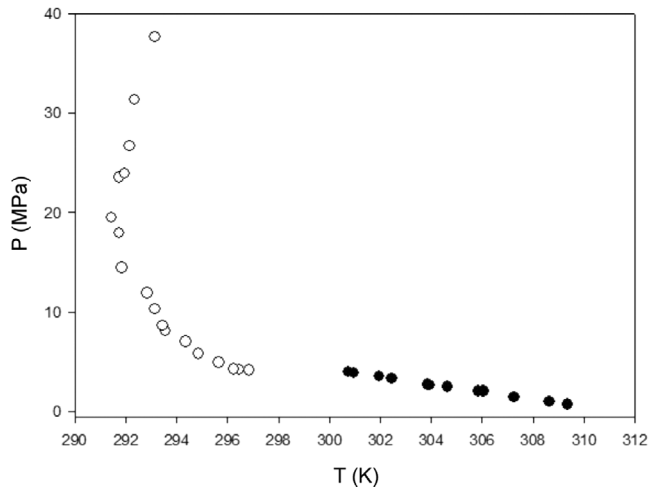

FIGURE 5 T – P Diagram for the SLG equilibrium of the CO_2+ lauric acid system: ● solid phase; ○ gas phase.

These measurements confirm the capability to generate reliable transport-property data at elevated pressures and to validate new viscometer designs, such as coil-type capillary viscosimeter coupled to vibrating-tube densimeters, the Figure 7 illustrate experimental dynamic viscosity data for THF at 313.15 K.

As expected, at constant temperature, viscosity increases with increasing pressure. At constant pressure, viscosity decreases with increasing temperature. Experimental data were determined up to 50 MPa and 353.15 K and are reported in Table 10.

4.5 | Hydrate dissociation in multicomponent systems

The dissociation conditions of gas hydrates for systems containing CO_2, water, and hydrocarbons, with and

TABLE 8 SLG equilibrium of the CO_2 + lauric acid system.

P (MPa)	T (K)	P (MPa)	T (K)
0.72	309.35	4.93	295.65
1.01	308.65	5.84	294.85
1.43	307.25	7.03	294.35
2.05	306.05	8.09	293.55
2.07	305.85	8.63	293.45
2.52	304.65	10.31	293.15
2.69	303.95	11.91	292.85
2.71	303.85	14.47	291.85
3.33	302.45	17.97	291.75
3.53	301.95	19.50	291.45
3.88	300.95	23.51	291.75
3.98	300.75	23.92	291.95
4.17	296.85	26.71	292.15
4.24	296.45	31.32	292.35
4.30	296.25	37.62	293.15

Note: Standard uncertainties u are $u(P) = 0.02$ MPa and $u(T) = 0.017$ K. The relative expanded uncertainty ($k = 2$) is estimated to be $Ur(x) = Ur(y) = 0.0196$.

TABLE 9 Liquid dynamic viscosity of CO_2 at 296.72 K.

T (K)	P (MPa)	η_{exp} (μPa s)
296.90	7.74	69.4
296.67	10.16	75.9
296.69	12.81	82.5
296.73	16.74	91.2
296.67	19.63	96.8
296.68	24.00	103.9
296.70	28.95	110.1

Note: Standard uncertainties u are $u(P) = 0.003$ MPa and $U(T) = 0.009$ K; the relative combined expanded uncertainty with a 0.95 level of confidence ($k = 2$) for viscosity is $U_{rc}\left(\eta_{exp}\right) = 0.010$.

without thermodynamic additives, were determined using isochoric, vacuum-insulated cells. Dissociation pressures and temperatures were obtained for systems with hydrocarbon mixtures and with promoters such as TBAB[48] and THF,[52] Figure 8. Within experimental uncertainty, the presence of alkanes such as hexane, decane, or dodecane has little effect on the hydrate stability region, whereas the addition of TBAB or THF shifts the dissociation curve to higher temperatures at a given pressure, consistent with their role as thermodynamic promoters or inhibitor.[48–52]

Table 11 reports experimentally determined hydrate dissociation points for the $H_2O(1) + C_6H_{14}$ ($w_2 = 0.0277$) + $C_{10}H_{22}$($w_3 = 0.0373$). These results contribute to the understanding of hydrate formation and inhibition in flow assurance and highlight the potential of hydrate-based technologies for gas storage and water treatment, where promoters and inhibitors must be carefully selected to balance performance and cost.

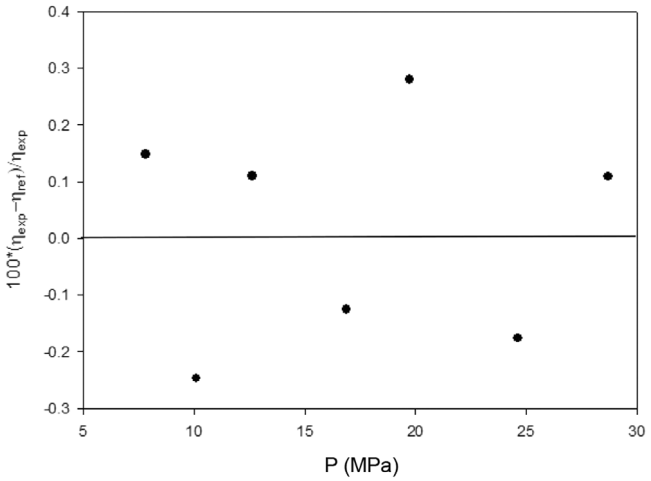

FIGURE 6 Experimental deviations for the dynamic viscosity of CO_2 at 296.72 K.

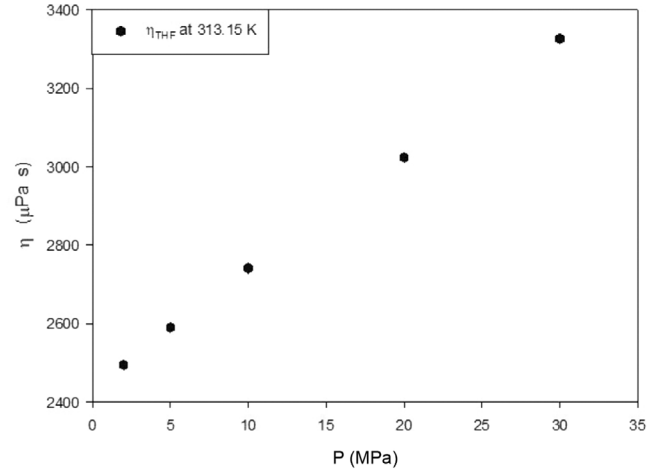

FIGURE 7 Liquid dynamic viscosity of THF at 313.15 K.

4.6 | Molecular simulations

The development of equations of state based on short-range interaction potentials was supported by extensive Monte Carlo and molecular dynamics simulations with systems of 512 particles for square-well and triangular-well fluids. Using ensembles such as NVT, NPT and Gibbs, as well as Gibbs–Duhem integration, the laboratory generated reference data for thermodynamic

properties and phase boundaries. The Barker–Henderson[62–64] perturbation theory up to fourth order was then employed to derive analytic expressions for the residual Helmholtz free energy[59] and related properties.[59–61]

TABLE 10 Experimental dynamic viscosity data for THF at 313.15 K.

P (MPa)	η (μPa s)
1.99	2495.3
5.00	2589.8
10.00	2741.0
20.00	3024.6
30.00	3327.0

Note: Standard uncertainties u are $u(P) = 0.002$ MPa and $u(T) = 0.009$ K; the relative combined expanded uncertainty with a 0.95 level of confidence ($k = 2$) for viscosity is $u_{rc}(\eta_{exp}) = 0.012$.

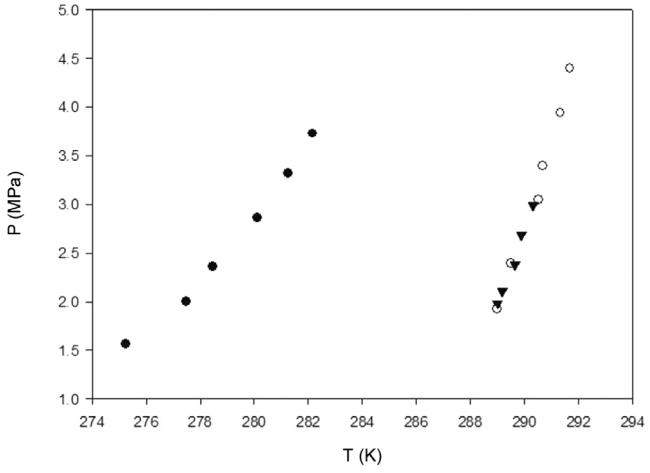

FIGURE 8 Experimental hydrate phase equilibria data ($H - L_w - L_h - V$) for $CO_2 + H_2O + C_6H_{14} + C_{10}H_{22} + C_{14}H_{30}$ + TBAB or THF Systems at $w_{mixture} = 0.1$: (○) $w_{TBAB} = 0.2$, (▲) $w_{THF} = 0.2$. Without thermodynamic promoter: (●) $w = 0.1$ (hydrocarbon mixture).

Figure 9 shows the results obtained for A_1 molecular simulation for the triangular well at lambdas less than 1.5, that is, for weak interactions. Only Solana at lambda of 1.3 has been published simulation data. The data under these conditions are compared with those published by Solana. Both data sets show the same trend and are consistent.

4.7 | Modelling and representative of experimental data

4.7.1 | VLE equilibrium

Phase equilibria data are of great importance for the chemical industry and for the development and/or validation of thermodynamic models, particularly, the supercritical fluid extraction depends of vapour–liquid and liquid–liquid equilibrium accurate data. VLE data and critical points for the $CO_2\,(1) + 1 - \text{propanol}\,(2)$ system are reported in Table 3, at 352.83 K.

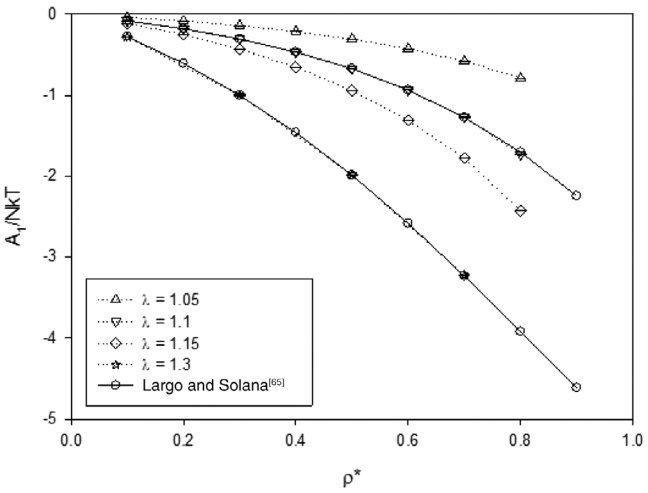

FIGURE 9 First order term in the perturbation theory for different values of $\lambda < 2$.

TABLE 11 Hydrate dissociation points data of the $H_2O\,(1) + C_6H_{14}(w_2 = 0.0277) + C_{10}H_{22}\ (w_3 = 0.0373) + C_{14}H_{30}(w_4 = 0.0350) +$ TBAB(5) or THF(5) systems.

w_2	w_3	w_4	P (MPa)	T (K)	w_{5TBAB}	P (MPa)	T (K)	w_{5THF}	P (MPa)	T (K)
0.0278	0.0371	0.0351	1.56	275.24	0.2	1.92	289.00	0.2	1.98	289.02
			2.00	277.48		2.39	289.52		2.11	289.20
			2.36	278.47		3.05	290.55		2.38	289.67
			2.86	280.12		3.40	290.67		2.69	289.90
			3.32	281.25		3.94	291.34		2.99	290.34
			3.73	282.15		4.40	291.69			

Note: Standard uncertainties u are $u(P) = 0.022$ MPa and $u(T) = 0.026$ K. The relative standard uncertainty is estimated to be $u_r(w_i) = 0.0009$.

Experimental VLE for the binary system are correlated using a Patel–Teja equation[13] with new extended Wong–Sandler[10,14] mixing rules (P-TM).

From the Patel-Teja equation:

$$P=\frac{RT}{v-b}-\frac{a}{v(v+b)+c(v-b)} \tag{1}$$

where the mixing rule proposed by Galicia et al.[10] is as follows:

$$\frac{a}{RT}=(3b+c)\frac{D}{2} \tag{2}$$

$$b=\frac{2Q+cD}{2-3D} \tag{3}$$

$$c=\sum x_i c_i \tag{4}$$

with:

$$D=\sum\frac{x_i a_i}{RT}\left(\frac{2}{3b_i+c_i}\right)-\frac{A_{ex}}{RT} \tag{5}$$

$$Q=\sum x_i x_j\left(b-\frac{a}{RT}\right)_{ij} \tag{6}$$

The activity coefficient model used in Equation (5) is the NRTL model.[62]

For this CO_2+1-propanol mixture, the parameters were optimized[10] using the experimental data reported in this work and are shown in the following table.

The VLE calculation algorithm was used in combination with the Marquardt–Lebenberg method, the binary interaction parameters were computed by minimizing the following objective function (OF):

$$\mathrm{OF}=\sum_{j=1}^{\mathrm{NP}}\left[\sum_{i=1}^{\mathrm{Nc}}\left(\frac{y_{ij}^{\mathrm{calcd}}-y_{ij}^{\mathrm{exptl}}}{y_{ij}^{\mathrm{exptl}}}\right)^2+\left(\frac{P_j^{\mathrm{calcd}}-P_j^{\mathrm{exptl}}}{P_j^{\mathrm{exptl}}}\right)^2\right] \tag{7}$$

where NP is the number of data points, Nc is the number of components, y is the vapour mole fraction, and the superscripts calcd and exptl denote the calculated and experimental values, respectively.

While the standard deviation in the vapour phase pressure and composition is 3.73 and 0.005, respectively, the results indicate that the deviations in pressure and composition are low.

4.7.2 | *PvT* properties

The experimental *PvT* data are presented in Table 4, and their behaviour is shown in Figure 2. The results show that, at a fixed pressure, density decreases as temperature increases. The *PvT* data are represented by the proposed empirical model, called the Galicia-Luna model with 5 parameters, which is easy to use due to its simplicity. An average deviation of 0.015% is obtained.

The density measurements of pure compounds in the pressure and temperature ranges were represented whit the five parameters empirical model proposed in this work by Galicia-Luna using Equation (8).

$$\rho_{\mathrm{cal}}=\frac{\left(\frac{a_3}{T}+\frac{a_4}{T^{\frac{1}{2}}}+\frac{a_5}{T^{\frac{1}{3}}}\right)+P}{a_1+a_2P} \tag{8}$$

where the calculated density is represented by ρ_{cal}. The parameters a_1, a_2, a_3, a_4 and a_5 are optimized by the Levenberg–Marquardt algorithm.[38]

In this work, the *PvT* properties of the H_2O+1 propanol system were measured using the latest equipment described above. In the case of increasing pressure at constant temperature, the density of the mixture increases.

The absolute average percentage deviation (AAPD) determines the accuracy of the parameter fit to the experimental data. Therefore, it was calculated using Equation (9), where N is the number of experimental data sets from the calibration method and ρ_{cal} is the density data calculated using the empirical model proposed by Galicia et al.,[16] the parameter of model, AAPD and MAPD are reported in Table 12. On the other hand, the maximum absolute percentage deviation (MAPD) was calculated using Equation (10).

$$\mathrm{AAPD}=\frac{100\sum_{i=1}^{n}\left|\frac{\rho_{\mathrm{F}}-\rho_{\mathrm{cal}}}{\rho_{\mathrm{F}}}\right|}{N} \tag{9}$$

TABLE 12 Parameters of the Galicia-Luna model and the absolute average percentage deviation (AAPD), and the maximum absolute percentage deviation (MAPD) for the representation of the density of a $H_2O\,(1)+1-$Propanol (2) mixture.

a_1 (MPa m^3 kg^{-1})	a_2 (m^3 kg^{-1})	a_3 (MPa K)	a_4 (MPa K$^{\frac{1}{2}}$)	a_5 (MPa K$^{\frac{1}{3}}$)	AAPD (%)	MAPD (%)
3.259313×10^{-1}	8.835498×10^{-2}	-2.306807×10^{5}	4.883317×10^{4}	-1.167029×10^{4}	0.015	0.028

$$\text{MAPD} = \max\left[100\left|\frac{\rho_F - \rho_{cal}}{\rho_F}\right|\right] \quad (10)$$

where max is the maximum value for this calculation and ρ_F is the experimentally determined density of the mixture.

4.7.3 | Viscosity

Capillary viscometers are the most commonly used instruments for measuring viscosity, especially in liquid phases. They are characterized by their simple structure and operation. They are commonly used for industrial measurements and research into the viscosity of liquids at atmospheric pressure, dense gases, and liquids at high pressures.[42]

The principle of capillary viscometers is based on Poiseuille's equation, formulated by Hagenbach based on experiments conducted in 1860 and between 1840 and 1846 by Poiseuille.[41] For laminar flow of a Newtonian fluid through a circular capillary tube, the viscosity η can be expressed in terms of the capillary radius (a), the tube length (L), the pressure drop in the tube (ΔP) and the volumetric flow rate (Q), as follows[42]:

$$\eta = \frac{\pi a^4 \Delta P}{8QL} \quad (11)$$

Equation (11) can be used to calculate the viscosity of any Newtonian fluid in straight capillary tubes. In the case of coiled capillary tubes, due to their configuration, Equation (11) does not represent the flow behaviour in a tube, since this equation is developed for a straight capillary tube. Therefore, based on the Navier–Stokes equations and the Hagen–Poiseuille equations, equations are derived for coiled capillary tubes, taking into account the loss of kinetic energy along the tube through which the fluid moves.[43,46]

$$\eta = \frac{\pi D^4}{256 Q_0 L P_0}\left(P_0^2 - P_L^2\right) \quad (12)$$

where Q_0 is the volumetric flow rate that depends on the pressure drop, P_0 and P_L are the pressures at the inlet and outlet of the capillary tube, respectively, D is the internal diameter of the capillary, and L is the length of the capillary. This equation takes into account compressibility effects under isothermal laminar flow conditions.

4.7.4 | Molecular simulations

Molecular simulations for short range square well potentials[58–65] are presented to continuation.

The square-well (SW) potential is as follows:

$$u(x) = \begin{cases} \infty & x \le 1 \\ -\varepsilon & 1 < x \le \lambda \\ 0 & \lambda < x \end{cases} \quad (13)$$

where $x = r/\sigma$ is the reduced distance, ε is the well depth, σ is the diameter of the hard core and λ is the range of the potential.

Based on the Barker and Henderson BH perturbation theory,[63] the residual Helmholtz free energy of a system of N particles at a fixed temperature can be expressed in terms of a series expansion in the inverse of the reduced temperature $T^* = kT/\varepsilon$ as follows:

$$\frac{A^{res}}{NkT} = \frac{A_0^{res}}{NkT} + \frac{1}{T^*}\frac{A_1}{NkT} + \frac{1}{T^{*2}}\frac{A_2}{NkT} + . \quad (14)$$

where the subscript 0 refers to the free energy of a reference system (taken to be a hard-sphere fluid), and A_i is the contribution of i^{th} order to the perturbation series. The first order term for the square-well potential is as follows:

$$\frac{A_1}{NkT} = 12\eta\int_0^\infty g_0(x)u_p^*(x)x^2dx \quad (15)$$

Results calculated by molecular dynamics simulations for short range square well potentials are presented in the next figure. The results at $\lambda = 1.3$ are compared with those published by Largo and Solana.[69]

5 | SCIENTIFIC, ACADEMIC, AND INDUSTRIAL IMPACT

Over the 28 years since the ESIQIE High-Pressure Thermodynamics Laboratory became fully operational, more than 88 theoretical and experimental articles have been published in international journals, covering experimental thermophysical properties, model development, and molecular simulation. The group has guest-edited special issues of Fluid Phase Equilibria devoted to thermophysical properties and phase equilibria, and has contributed to special issues of the Journal of Chemical and Engineering Data, including the Latin America issue and a High-Impact Authors issue. These activities reflect the

integration of the laboratory into the international thermodynamics community.[4–9]

Collaborations with groups led by S. I. Sandler, J. Gmehling, D. Richon, A. H. Mohammadi, and T. de Loos, among others, have played a central role in methodological development and model assessment. Joint work has ranged from mixing-rule development and equation-of-state formulation to hydrate phase equilibria and supercritical extraction.

More than 80 students have completed bachelor's, master's, or doctoral theses in the laboratory, many of them now active in academia and industry, national and international. Several graduates are members of the Mexican National System of Researchers at different levels, while others have received national and international awards. Although academic genealogy is not the main focus of this article, it is an important mechanism through which methodological know-how and scientific culture in thermodynamics are transferred to new institutions and industrial sectors.

The experimental and modelling work summarized here has been motivated by concrete process-engineering questions in the petroleum, chemical, food and environmental sectors. For example, supercritical extraction studies for natural products such as carotenoids, boldine, vanilla components, and squalene provide property data and correlations used in the design and optimization of extraction units.[66–69] Hydrate phase equilibrium data for CO_2 + water systems with promoters and inhibitors support the evaluation of hydrate-based technologies for gas storage and for the removal of contaminants from water.[48–52] High-pressure viscosity and density data for polar and non-polar fluids contribute to more reliable pipeline design and to the assessment of transport models used in reservoir and process simulators.[16–26]

6 | CHALLENGES IN THERMODYNAMICS FOR CHEMICAL ENGINEERING

Despite significant progress, several challenges remain in thermodynamics as applied to chemical engineering. First, there is a need for equations of state capable of describing the critical region and compressed-liquid volumes of complex mixtures with relative errors well below 1%, while remaining tractable for process simulation. Second, the design of separation processes that minimize environmental impact will increasingly rely on non-conventional approaches such as supercritical fluids, gas hydrates, and other alternative working fluids, which require reliable thermophysical-property data over wide ranges of conditions. Third, integrated experimental–modelling infrastructures that cover the full scale from laboratory to pilot and industrial plants are needed to translate advances in thermodynamics into industrial practice.[66–69]

7 | CONCLUSIONS

Between 1990 and 2025, the High-Pressure Thermodynamics Laboratory at ESIQIE-IPN has evolved from a newly created facility into a mature research group recognized for its contributions to thermophysical-property measurements, model development and molecular simulation. By organizing the discussion around scientific questions and methodological innovations rather than institutional milestones, this article has highlighted six major research lines: high-pressure phase equilibria, volumetric properties, solubilities, and supercritical extraction, viscosities, hydrate equilibria, and equations of state supported by simulation. Representative case studies demonstrate how experimental data, empirical correlations, and molecular-based models have been combined to address problems in chemical, petroleum, food, and environmental engineering. The thermodynamic research laboratory in Mexico from 1997, applied to accurate experimental determination of thermodynamic and transport fluid properties of fluids, solids and his mixtures up to 100 MPa and 673 K.

The laboratory's impact extends beyond its publications: it includes the training of highly qualified personnel, the development of unique experimental infrastructure in Mexico, and the establishment of international collaborations. Looking forward, advances in accurate equations of state for complex mixtures, environmentally benign separations, and multi-scale modelling will continue to require high-quality thermophysical data and integrated experimental–theoretical efforts. The experience summarized here illustrates how a focused high-pressure thermodynamics program can contribute to these goals. Finally, through 28 years of thermophysical measurements, the Thermodynamics Laboratory has contributed to the scientific, research, and technological community with the determination of thermophysical properties with high accuracy for the development of processes without environmental impact.

NOMENCLATURE

Variables

A_{ex}	excess Helmholtz free energy
A^{res}	residual Helmholtz free energy
G^{ex}	excess Gibbs free energy
L_h	liquid hydrocarbon phase
L_w	liquid water phase
P_0	pressure at the inlet of the capillary tube
P_L	pressure at the outlet of the capillary tube
P_c	critical pressure

P_j^{calcd}	calculated pressure
P_j^{exptl}	experimental pressure
Q_0	volumetric flow rate referenced to P_0
T_c	critical temperature
a_1, a_2, a_3, a_4, a_5	parameters of Galicia − Luna model
a_i, b_i, c_i	interaction parameters for species i
$k_{12}, \tau_{12}, \tau_{21}, \alpha_{12}$	parameters of NRTL model correlated to the binary mixture CO_2 (1)+1−Propanol (2)
u_c	combined uncertainties
u_r	relative expanded uncertainty
w_1, w_2, w_3, w_4	component 1, 2, 3 or 4 mass fractions
$w_{mixture}$	mixture mass fraction
w_{TBAB}	TBAB mass fraction
w_{THF}	THF mass fraction
x_c	critical composition
x_i	liquid molar fraction of species i
x_j	liquid molar fraction of species j
y_{ij}^{calcd}	calculated molar fraction of vapour
y_{ij}^{exptl}	experimental molar fraction of vapour
η_{cal}	calculated dynamic viscosity
η_{exp}	experimental dynamic viscosity
ρ_{cal}	calculated density
ρ_{exp}	experimental density
ρ^{Liq}	liquid density
ρ^{Vap}	vapour density
ρ_F	fluid density
ΔP	pressure drop across the capillary
AAPD	absolute average percentage deviation
MAPD	maximum absolute percentage deviation
D	capillary internal diameter
H	hydrate phase
L	capillary length
N	number of experimental data points
P	pressure
Q	volumetric flow rate
T	temperature
V	vapour phase
a	capillary radius
a, b, c	interaction parameters
k	Boltzmann constant
u	standard uncertainty
x	molar fraction of the liquid
x	reduced distance
y	molar fraction of the vapour
ε	well depth
η	dynamic viscosity
λ	range of the potential
ρ	density
σ	diameter of the hard core

AUTHOR CONTRIBUTIONS

Luis A. Galicia-Luna: Conceptualization; investigation; funding acquisition; writing – original draft; methodology; validation; writing – review and editing; visualization; resources; formal analysis.

ACKNOWLEDGEMENTS

The author thanks the National Polytechnic Institute, ESIQIE, and CONACyT (SECIHTI) for their financial support during this research. Special thanks are extended to the former directors of ESIQIE (Eng. Timoteo Pastrana Aponte†) and the Department of Postgraduate Studies and Research (Prof. Jose Enrique Villa Rivera) for their interest, vision, and support, which were fundamental for the creation of the Experimental Thermodynamics Laboratory. Thanks to Cesar Rodriguez-Guerrero, Deputy Director of Educational Services, for his assistance with the statistics on chemical engineering graduates from ESIQIE. The author gives special thanks to his advisors, doctoral, D. Richon (Ecole Nationale des Mines de Paris), and bachelor in physics, A. Mondragon-Ballesteros† (from the physics institute of UNAM). Finally, thanks to all my former students, especially Mariana I Iturbe-Rodriguez (BSc) and Cristofher A. Arroyo-Hermández (PhD) for their valuable help.

PEER REVIEW

For transparency, the peer review documents associated with this article are available at https://doi.org/10.1002/cjce.70415.

DATA AVAILABILITY STATEMENT

Research data are not shared.

ORCID

Luis A. Galicia-Luna https://orcid.org/0000-0003-1862-8499

REFERENCES

[1] L. A. Galicia, D. Richon, T. W. de Loos, *Proceedings of the Thermodynamics Session, Organized in Honor of Professor Stanley I. Sandler at the 5th International Symposium of the E.S.I.Q.I.E.*, Vol. 210, Fluid Phase Equilibria Journal, Mexico City, Mexico **2003**, p. 2.

[2] L. A. Galicia, D. Richon, T. W. de Loos, *Fluid Phase Equilib.* **2007**, *259*, 1.

[3] L. A. Galicia-Luna, T. W. de Loos, H. V. Kehiaian, *Fluid Phase Equilib.* **2010**, *296*, 1.

[4] L. A. Galicia, A. Pimentel, J. J. Castro, A. M. Notario, C. Sánchez, P. Esquivel, *J. Chem. Eng. Data* **2019**, *64*, 2075.

[5] M. Christov, R. Dohrn, *Fluid Phase Equilib.* **2002**, *202*, 153.

[6] R. Dohrn, S. Peper, J. M. S. Fonseca, *Fluid Phase Equilib.* **2010**, *288*, 1.

[7] J. M. S. Fonseca, R. Dohrn, S. Peper, *Fluid Phase Equilib.* **2011**, *300*, 1.

[8] S. Peper, J. M. S. Fonseca, R. Dohrn, *Fluid Phase Equilib.* **2019**, *484*, 126.

[9] R. Dohrn, S. Peper, C. Secuianu, J. M. S. Fonseca, *Fluid Phase Equilib.* **2024**, *579*, 113978.

[10] L. A. Galicia, A. Ortega, D. Richon, *J. Chem. Eng. Data* **2000**, *45*, 265.

[11] A. Ortega, *Master Thesis*, Instituto Politécnico Nacional (CDMX, México) **1998**.
[12] J. L. Mendoza, *Master Thesis*, Instituto Politécnico Nacional (CDMX, México) **1998**.
[13] N. C. Patel, A. S. Teja, *Chem. Eng. Sci.* **1982**, *37*, 463.
[14] D. S. H. Wong, S. I. A. Sandler, *AIChE J.* **1992**, *38*, 671.
[15] L. A. Galicia-Luna, O. Elizalde, *Fluid Phase Equilib.* **2010**, *296*, 46.
[16] L. A. Galicia-Luna, D. Richon, H. Renon, *J. Chem. Eng. Data* **1994**, *39*, 424.
[17] L. A. Galicia, *PhD Thesis*, École nationale supérieure des mines de Paris (Paris, France) **1990**.
[18] A. Zúñiga, *Master Thesis*, Instituto Politécnico Nacional (CDMX, México) **1999**.
[19] A. Zúñiga, L. A. Galicia, *J. Chem. Eng. Data* **2002**, *47*, 155.
[20] A. Zúñiga, L. A. Galicia, *J. Chem. Eng. Data* **2002**, *47*, 149.
[21] R. Quevedo, L. A. de la Cruz, L. A. Galicia, O. Elizald, *J. Chem. Eng. Data* **2011**, *56*, 4226.
[22] R. Quevedo, L. A. Galicia, O. Elizalde, *J. Chem. Thermodyn.* **2012**, *44*, 133.
[23] M. A. Viascan, *Bachelor Thesis*, Instituto Politécnico Nacional (CDMX, México) **2004**.
[24] R. Jimenez, *Bachelor Thesis*, Instituto Politécnico Nacional (CDMX, México) **2005**.
[25] R. P. Mendo, A. Pimentel, A. Ruiz, L. A. Galicia, *J. Chem. Eng. Data* **2023**, *68*, 3265.
[26] R. P. Mendo, A. Pimentel, A. M. Notario, L. A. Galicia, *J. Chem. Thermodyn.* **2024**, *192*, 107250.
[27] L. E. Camacho, *Master Thesis*, Instituto Politécnico Nacional (CDMX, México) **2003**.
[28] A. Zúñiga, *PhD Thesis*, Instituto Politécnico Nacional (CDMX, México) **2006**.
[29] V. Serrano, *Master Thesis*, Instituto Politécnico Nacional (CDMX, México) **2003**.
[30] V. H. Soto, *Master Thesis*, Instituto Politécnico Nacional (CDMX, México) **2009**.
[31] M. S. Duran, *Master Thesis*, Instituto Politécnico Nacional (CDMX, México) **2012**.
[32] A. Rojas, *PhD Thesis*, Instituto Politécnico Nacional (CDMX, México) **2016**.
[33] A. Rojas, A. Pimentel, T. Rosales, G. Dávila, L. A. Galicia, *J. Chem. Eng. Data* **2016**, *61*, 3225.
[34] R. Garcia, *Master Thesis*, Instituto Politécnico Nacional (CDMX, México) **2012**.
[35] T. Rosales, *PhD Thesis*, Instituto Politécnico Nacional (CDMX, México) **2017**.
[36] T. Rosales, C. Jiménez, A. Cardador, S. Teresita, L. A. Galicia, D. I. Téllez, G. Dávila, *J. Food Qual.* **2017**, *1*, 6879712.
[37] C. Sánchez, *Master Thesis*, Instituto Politécnico Nacional (CDMX, México) **2012**.
[38] A. Zúñiga, L. A. Galicia, L. E. Camacho, *Fluid Phase Equilib.* **2005**, *234*, 151.
[39] J. Romero, *Master Thesis*, Instituto Politécnico Nacional (CDMX, México) **1995**.
[40] J. M. Bernal, L. A. Galicia, K. R. Hall, M. Ramos, G. A. Iglesias, *J. Chem. Eng. Data* **2004**, *49*, 864.
[41] A. Pimentel, *PhD Thesis*, Instituto Politécnico Nacional (CDMX, México) **2015**.
[42] A. Pimentel, L. A. Galicia, J. J. Castro, *J. Chem. Eng.* **2016**, *61*, 45.
[43] R. P. Mendo, *PhD Thesis*. Instituto Politécnico Nacional (CDMX, México) 2020.
[44] R. P. Mendo, A. Ruiz, A. Pimentel, L. A. Galicia, *J. Chem. Thermodyn.* **2022**, *172*, 106830.
[45] A. Ruiz, A. Pimentel, R. P. Mendo, L. A. Galicia, *J. Chem. Eng. Data* **2022**, *67*, 3589.
[46] R. P. Mendo, C. A. Arroyo, A. Pimentel, L. A. Galicia, *Fluid Phase Equilib.* **2020**, *515*, 112559.
[47] C. A. Arroyo, *Master Thesis*, Instituto Politécnico Nacional (CDMX, México) **2024**.
[48] V. Belandria, A. H. Mohammadi, A. Eslamimanesh, D. Richon, M. F. Sánchez, L. A. Galicia, *Fluid Phase Equilib.* **2012**, *322–323*, 105.
[49] M. F. Sánchez, *Master Thesis*, Instituto Politécnico Nacional (CDMX, México) **2012**.
[50] M. F. Sanchez, L. A. Galicia, A. Pimentel, A. H. Mohammadi, *J. Chem. Eng. Data* **2019**, *64*, 763.
[51] J. M. Chima, P. Esquivel, A. Pimentel, L. A. Galicia, J. J. Castro, *J. Chem. Eng. Data* **2019**, *64*, 4775.
[52] N. L. Ramírez, A. Pimentel, L. A. Galicia, A. M. Notario, *J. Chem. Thermodyn.* **2022**, *168*, 106750.
[53] J. C. Guevara, E. Severiano, *Bachelor Thesis*, Instituto Politécnico Nacional (CDMX, México) **1992**.
[54] I. Rojas, *Master Thesis*, Instituto Politécnico Nacional (CDMX, México) **1996**.
[55] G. N. Escobedo, *Bachelor Thesis*, Instituto Politécnico Nacional (CDMX, México) **1995**.
[56] S. Lopez, *Master Thesis*, Instituto Politécnico Nacional (CDMX, México) **1996**.
[57] N. L. Diaz, *Master Thesis*, Instituto Politécnico Nacional (CDMX, México) **2000**.
[58] F. F. Betancourt, *Master Thesis*, Instituto Politécnico Nacional (CDMX, México) **2004**.
[59] F. F. Betancourt, L. A. Galicia, S. I. Sandler, *Mol. Phys.* **2007**, *105*, 2987.
[60] F. F. Betancourt, *PhD Thesis*, Instituto Politécnico Nacional (CDMX, México) **2008**.
[61] F. F. Betancourt, L. A. Galicia, A. L. Benavides, J. A. Ramírez, E. Schöll, *Mol. Phys.* **2008**, *106*, 113.
[62] J. A. Barker, D. Henderson, *J. Chem. Phys.* **1967**, *47*, 2856.
[63] W. R. Smith, D. Henderson, J. A. Barker, *J. Chem. Phys.* **1971**, *55*, 4027.
[64] J. A. Barker, D. Henderson, *Rev. Mod. Phys.* **1976**, *48*, 587.
[65] J. Largo, J. R. Solana, *Mol. Sim.* **2003**, *29*, 363.
[66] G. M. Kontogeorgis, R. Dohrn, I. G. Economou, J. C. de Hemptinne, A. ten Kate, S. Kuitunen, M. Mooijer, L. F. Žilnik, V. Vesovic, *Ind. Eng. Chem. Res.* **2021**, *60*, 4987.
[67] J. D. Seader, E. J. Henley, D. K. Roper, *Separation Process Principles Chemical and Biochemical Operation*, 3rd ed., John Wiley & Sons, Hoboken, NJ **2010**, p. 8.
[68] J. C. de Hemptinne, G. M. Kontogeorgis, R. Dohrn, I. G. Economou, A. ten Kate, S. Kuitunen, L. F. Žilnik, M. G. De Angelis, V. Vesovic, *Ind. Eng. Chem. Res.* **2022**, *61*, 14664.
[69] O. V. Kashurin, V. I. Deshchenya, N. D. Kondratyuk, *Fluid Phase Equilib.* **2025**, *589*, 114244.
[70] C. Garlapati, G. Madras, *J. Chem. Eng. Data* **2008**, *53*, 2637.

How to cite this article: L. A. Galicia-Luna, *Can. J. Chem. Eng.* **2026**, 1. https://doi.org/10.1002/cjce.70415